arXiv:1602.07173v2 [astro-ph.SR] 3 May 2016

Frequency Redistribution of Polarized Light in the Λ-Type Multi-Term Polarized Atom

R. Casini[a] and R. Manso Sainz[b]

[a] *High Altitude Observatory, National Center for Atmospheric Research,*[1]
P.O. Box 3000, Boulder, CO 80307-3000, U.S.A.

[b] *Max-Planck-Institut für Sonnensystemforschung,*
Justus-von-Liebig-Weg 3, 37077 Göttingen, Germany

ABSTRACT

We study the effects of Rayleigh and Raman scattering on the formation of polarized spectral lines in a Λ-type multi-term atom. We fully take into account the partial redistribution of frequency and the presence of atomic polarization in the lower states of the atomic model. Problems that can be modeled with this formalism include, for example, the formation of the Ca II H-K and IR triplet, the analogous system of Ba II, and the Lyβ-Hα system of hydrogenic ions.

1. Introduction

Many resonance lines of the solar spectrum show complex linear polarization patterns, especially when observed near the solar limb (Wiehr 1975; Stenflo & Keller 1996, 1997; Stenflo, Keller, & Gandorfer 2000; Gandorfer 2002). These signals are generated by scattering in the upper photosphere and chromosphere, where the plasma is very rarefied and nearly collisionless, and long integration paths are involved in the production of the observed polarized signals. Under these conditions, the ground state of the observed transitions may harbour a significant amount of atomic polarization (Trujillo Bueno & Landi Degl'Innocenti 1997; Trujillo Bueno et al. 2002; Manso Sainz & Trujillo Bueno 2003), and coherence effects among the atomic levels become apparent in the emergent polarization profiles (e.g., Stenflo 1980, 1997; Landi Degl'Innocenti 1998; Casini & Manso Sainz 2005; Belluzzi & Trujillo Bueno 2011; Smitha et al. 2012)

A general expression for the *second-order emissivity* describing coherent[2] resonance scattering in a two-term polarized atom was recently presented by Casini et al. (2014; hereafter, Paper I). On the other hand, very few lines in the solar spectrum can be considered strictly resonant. The ions in the solar atmosphere are illuminated by a broadband radiation field that pumps the atomic levels through all possible transitions simultaneously, creating many different scattering channels. These conditions are responsible for the appearance of complex coherence phenomena, where the

[1] The National Center for Atmospheric Research is sponsored by the National Science Foundation.

[2] Following the terminology already adopted in Paper I, here we use the term "coherent" in the broader sense of "memory preserving", rather than in the traditional sense of "frequency preserving". The latter meaning will instead be implied when describing the results of Section 3.

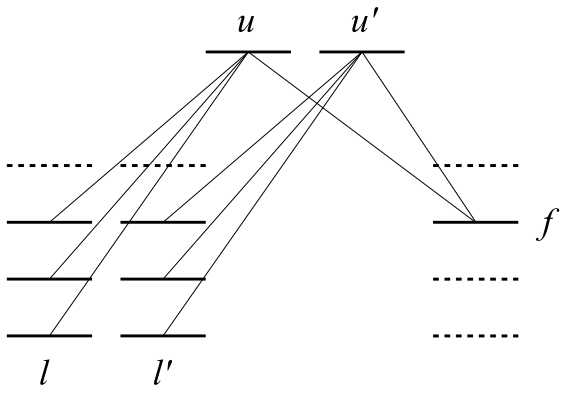

Fig. 1.— Schematic diagram of the Λ-type, multi-term model atom considered in this paper, which is relevant for the modeling of the polarization of the $u \rightarrow f$ transition. In order to correctly describe the polarization properties of the outgoing light, all lower terms (l, l') that are radiatively connected to the (virtual) upper term (u, u'), also including the final term f, must be taken into account. Our model is restricted to the case where all (l, l') levels are sharp (i.e., with practically infinite lifetime).

scattered polarization signatures become coupled with the atomic polarization of the various energy levels involved in the atomic transitions. The expression that was presented in Paper I for the two-term atom is general enough that it lends itself to a straightforward extension to the treatment of more complex atomic structures. Here we generalize such expression to the description of polarized radiation effects in a Λ-type multi-term atom, where the lower terms of the system are all radiatively coupled to a common excited state (see Figure 1).

An important example of such Λ-type system is contained in the Ca II ion, and underlies the formation of some notable transitions observed in the solar spectrum: the H and K lines around 395 nm, which display a complex polarization pattern spanning more than 10 nm (Stenflo 1980; Stenflo, Baur, & Elmore 1980; Gandorfer 2002), due to coherent scattering and quantum interference between the levels of the upper ^2P term of the doublet (Stenflo 1980); and the infrared (IR) triplet around 858 nm, in particular the 854.2 nm and 866.2 nm lines, which under solar conditions is dominated by the presence of atomic polarization in the metastable ^2D term (Manso Sainz & Trujillo Bueno 2001, 2003). The UV doublet and the IR triplet are connected via the common ^2P upper term, yet previous attemps at modeling the formation of these sets of lines have not taken into account the full complexity of this system: either coherent scattering in a multi-level system was considered, but the essential polarization of the metastable ^2D levels was neglected (Sampoorna, Nagendra, & Stenflo 2013), or the atomic polarization of all the levels was included in the modeling of the IR triplet pattern, but coherence effects among the levels of the upper ^2P term were neglected (Manso Sainz & Trujillo Bueno 2001, 2003).

In the next Section, we provide explicit expressions for the Λ-type multi-term atom with and without hyperfine structure, as well as for the multi-level atom, when the fine-structure interaction

is completely neglected. Finally, in Section 3 we present the application of this formalism to the modeling of the polarized line profiles of some notable Λ-type atomic systems.

2. The Λ-type multi-term polarized atom with hyperfine structure

We consider the general form of the radiative transfer equation for polarized light in spectral lines, including the process of coherent scattering in a spectral line, which is responsible for the effects of partial redistribution of the radiation frequency when the illumination of the atom is not spectrally flat. Such transfer equation was presented in Casini et al. (2014) (hereafter, Paper I), and when the polarized radiation is expressed in terms of the Stokes vector $\boldsymbol{S} \equiv (S_0, S_1, S_2, S_3) \equiv (I, Q, U, V)$, it takes the form

$$\frac{1}{c}\frac{d}{dt} S_i(\omega_{k'}, \hat{\boldsymbol{k}}') = -\sum_j \kappa_{ij}(\omega_{k'}, \hat{\boldsymbol{k}}')\, S_j(\omega_{k'}, \hat{\boldsymbol{k}}') + \varepsilon_i^{(1)}(\omega_{k'}, \hat{\boldsymbol{k}}') + \varepsilon_i^{(2)}(\omega_{k'}, \hat{\boldsymbol{k}}') \; . \qquad (i = 0, 1, 2, 3) \quad (1)$$

Here κ_{ij} is the absorption matrix (corrected for radiation stimulated effects), and $\varepsilon_i^{(1)}$ and $\varepsilon_i^{(2)}$ are the source terms due to the spontaneous emission of radiation from the excited levels, and to coherent scattering in the spectral line, respectively.

In the particular case of sharp lower levels, and in the absence of collisions, there is no true excitation of the upper levels, because of the infinite radiative lifetime of the lower levels. Then, the emissivity due to the spontaneous emission term $\varepsilon_i^{(1)}$ in the transfer equation can be neglected, as well as stimulation effects of the radiation (see Paper I). In this case, the absorption term does not originate from true photon absorption, but corresponds instead to the atom's cross-section for the coherent scattering of radiation.

Accordingly, in this work we consider the scattering of radiation in resonance lines when both the initial and final states of the transition are infinitely sharp. Then the only *positive* contribution to the line radiation comes from the coherent scattering term $\varepsilon_i^{(2)}$. This is given by Equation (I.20),

$$\begin{aligned}\varepsilon_i^{(2)}(\omega_{k'}, \hat{\boldsymbol{k}}') \equiv \frac{4}{3}\frac{e_0^4}{\hbar^2 c^4}\mathcal{N}\omega_{k'}^4 \sum_{ll'}\rho_{ll'}\sum_{uu'f}\sum_{qq'}\sum_{pp'}(-1)^{q'+p'}\,(r_q)_{ul}(r_{q'})^*_{u'l'}(r_p)_{u'f}(r_{p'})^*_{uf} \qquad (2)\\ \times\sum_{KQ}\sum_{K'Q'}\sqrt{(2K+1)(2K'+1)}\begin{pmatrix}1 & 1 & K\\ -q & q' & -Q\end{pmatrix}\begin{pmatrix}1 & 1 & K'\\ -p & p' & -Q'\end{pmatrix}T^{K'}_{Q'}(i, \hat{\boldsymbol{k}}')\\ \times\int_0^\infty d\omega_k\left(\Psi^{-k,+k'-k}_{u'l',ful} + \bar{\Psi}^{-k,+k'-k}_{ul,fu'l'}\right)J^K_Q(\omega_k)\; . \qquad (i = 0, 1, 2, 3)\end{aligned}$$

Here, $e_0(r_q)_{ab}$ represents the matrix element between the atomic states a and b of the q spherical component of the electric dipole moment, $e_0\boldsymbol{r}$. The geometric tensors $T^K_Q(i, \hat{\boldsymbol{k}})$ were introduced by Landi Degl'Innocenti (1984), and their algebraic expressions have been tabulated by several authors (e.g., Bommier 1997; Landi Degl'Innocenti & Landolfi 2004). The radiation tensors $J^K_Q(\omega_k)$ are defined in terms of these geometric tensors and the incident Stokes vector as follows,

$$J^K_Q(\omega_k) = \oint \frac{d\hat{\boldsymbol{k}}}{4\pi}\sum_{j=0}^{3} T^K_Q(j, \hat{\boldsymbol{k}})\, S_j(\omega_k, \hat{\boldsymbol{k}}) \; . \qquad (3)$$

Table 1: Notable Λ-type multiplets of the polarized solar spectrum observed near the limb (see, e.g. Stenflo et al 1983a,b; Gandorfer 2000, 2002, 2005)

Ion	λ (nm)	lower terms	upper term
H I	102.5 (Lyβ)	$1s\ ^2S$	$3p\ ^2P^\circ$
	656.3 (Hα)	$2s\ ^2S$	
Ca II	393.4 (K), 396.8 (H)	$4s\ ^2S$	$4p\ ^2P^\circ$
	849.8, 854.2, 866.2	$3d\ ^2D$	
Ba II	455.4 (D_2), 493.4 (D_1)	$6s\ ^2S$	$6p\ ^2P^\circ$
	585.4, 614.2, 649.7	$5d\ ^2D$	
Sc II	424.7	$3p^6 3d4s\ ^1D$	$3p^6 3d4p\ ^1D^\circ$
	660.5	$3p^6 3d^2\ ^1D$	
Cr I	520.4, 520.6, 520.8	$a\ ^5S$	$z\ ^5P^\circ$
	524.7, . . . , 540.9	$a\ ^5D$	
	2017.9. . . 2024.6	$a\ ^5P$	

Finally, the profiles $\Psi_{ab,cde}^{\pm h,\pm k\pm l}$, which describe the effects of frequency redistribution, are given by Equation (I.5). We indicate the complex conjugate of these profiles with $\bar{\Psi}_{ab,cde}^{\pm h,\pm k\pm l}$.

Equation (2) describes the scattering of polarized light that occurs in the radiative transition from a set of lower levels (l, l') – weighted by the density matrix $\rho_{ll'}$ and the gas density $\mathcal{N}$ for the ionic species considered – to a final set of levels f, via the virtual excitation of a set of intermediate upper levels (u, u'). It is important to observe that this expression generally describes the scattering polarization of a radiative transition $u \to f$ that results from the combination of distinct Λ-type atomic systems sharing the same final branch $(u, u') \to f$, but with different initial branches $(l, l') \to (u, u')$ (see Figure 1). Therefore, Equation (2) can be used to model the scattering of polarized radiation in multi-term atoms of the Λ-type, including the effects of a magnetic field and of lower-level polarization. We consider the general case where the hyperfine structure may be present, since such a model is necessary to describe many interesting spectral lines of the solar chromosphere (see Table 1).

We must observe that the index substitution $l'' \to f$ in the original expression (I.20) for the second-order emissivity of a two-term atom, which allowed us to write equation (2), is not just a formal exercise. There are supporting physical arguments showing that this new expression actually applies to the case of a Λ-type multi-term atom. For example, it reproduces the spectral emission of such a system when the incident radiation field is spectrally flat, i.e., in the limit of complete redistribution of the incident energy (see Paper I, Sect. 6). This correct behavior was numerically verified in all atomic models that we tested.

We indicate with α_l and α_f the electronic configuration of the two lower terms representing respectively the initial and final states of the transition, and correspondingly with α_u the electronic

configuration of the intermediate upper term (see Figure 1). We assume the direction of the magnetic field as the quantization axis (z-axis). Then the atomic states involved in Equation (1) are of the form

$$\begin{aligned} l &\equiv \alpha_l I \mu_l M_l \ , \quad l' \equiv \alpha_l I \mu'_l M'_l \ , \\ u &\equiv \alpha_u I \mu_u M_u \ , \quad u' \equiv \alpha_u I \mu'_u M'_u \ , \\ f &\equiv \alpha_f I \mu_f M_f \ , \end{aligned}$$

where M is the projection of the total angular momentum $\boldsymbol{F}$ on the z-axis, I is the quantum number of the nuclear spin, while μ is the index of the atomic Hamiltonian eigenbasis spanning the subspace of all the quantum numbers J and F that are associated with a given value of M.

Following the formalism of Paper I, Equation (2) becomes

$$\begin{aligned} \varepsilon_i^{(2)}(\omega_{k'}, \hat{\boldsymbol{k}}') = \frac{3}{16\pi^3} \mathcal{N} \hbar \, \omega_{k'}^4 \, \Pi_{L_u}^2 \frac{A_{uf}}{\omega_{uf}^3} \sum_{L_l} \Pi_{L_l}^2 B_{lu} \qquad (4) \\ \times \sum_{J_u J'_u J''_u J'''_u} \sum_{J_l J'_l J_f J'_f} \sum_{F_u F'_u F''_u F'''_u} \sum_{F_l F'_l F_f F'_f} (-1)^{J_u + J'_u + J''_u + J'''_u} (-1)^{J_l + J'_l + J_f + J'_f} \\ \times \Pi_{J_u J'_u J''_u J'''_u} \, \Pi_{J_l J'_l J_f J'_f} \begin{Bmatrix} J_u & J_l & 1 \\ L_l & L_u & S \end{Bmatrix} \begin{Bmatrix} J'_u & J'_l & 1 \\ L_l & L_u & S \end{Bmatrix} \begin{Bmatrix} J''_u & J_f & 1 \\ L_f & L_u & S \end{Bmatrix} \begin{Bmatrix} J'''_u & J'_f & 1 \\ L_f & L_u & S \end{Bmatrix} \\ \times \Pi_{F_u F'_u F''_u F'''_u} \, \Pi_{F_l F'_l F_f F'_f} \begin{Bmatrix} F_u & F_l & 1 \\ J_l & J_u & I \end{Bmatrix} \begin{Bmatrix} F'_u & F'_l & 1 \\ J'_l & J'_u & I \end{Bmatrix} \begin{Bmatrix} F''_u & F_f & 1 \\ J_f & J''_u & I \end{Bmatrix} \begin{Bmatrix} F'''_u & F'_f & 1 \\ J'_f & J'''_u & I \end{Bmatrix} \\ \times \sum_{\mu_u M_u} \sum_{\mu'_u M'_u} \sum_{\mu_f M_f} C_{\mu_u}^{J_u F_u}(M_u) \, C_{\mu_u}^{J''_u F''_u}(M_u) \, C_{\mu'_u}^{J'_u F'_u}(M'_u) \, C_{\mu'_u}^{J'''_u F'''_u}(M'_u) \, C_{\mu_f}^{J_f F_f}(M_f) \, C_{\mu_f}^{J'_f F'_f}(M_f) \\ \times (\epsilon_{uu'} + \mathrm{i}\omega_{uu'})^{-1} \sum_{\bar{J}_l \bar{J}'_l} \sum_{\bar{F}_l \bar{F}'_l} \sum_{\mu_l M_l} \sum_{\mu'_l M'_l} C_{\mu_l}^{J_l F_l}(M_l) \, C_{\mu_l}^{\bar{J}_l \bar{F}_l}(M_l) \, C_{\mu'_l}^{J'_l F'_l}(M'_l) \, C_{\mu'_l}^{\bar{J}'_l \bar{F}'_l}(M'_l) \\ \times \sum_{KQ} \sum_{K'Q'} \sum_{K_l Q_l} \sum_{qq'} \sum_{pp'} (-1)^{\bar{F}_l - M_l + q' + p'} \begin{pmatrix} 1 & 1 & K \\ -q & q' & -Q \end{pmatrix} \begin{pmatrix} 1 & 1 & K' \\ -p & p' & -Q' \end{pmatrix} \begin{pmatrix} \bar{F}_l & \bar{F}'_l & K_l \\ M_l & -M'_l & -Q_l \end{pmatrix} \\ \times \begin{pmatrix} F_u & F_l & 1 \\ -M_u & M_l & q \end{pmatrix} \begin{pmatrix} F'_u & F'_l & 1 \\ -M'_u & M'_l & q' \end{pmatrix} \begin{pmatrix} F'''_u & F'_f & 1 \\ -M'_u & M_f & p \end{pmatrix} \begin{pmatrix} F''_u & F_f & 1 \\ -M_u & M_f & p' \end{pmatrix} \\ \times \Pi_{KK'K_l} \, T_{Q'}^{K'}(i, \hat{\boldsymbol{k}}') \, \rho_{Q_l}^{K_l}(\bar{J}_l \bar{F}_l, \bar{J}'_l \bar{F}'_l) \\ \times \sum_{j=0}^{3} \oint \frac{d\hat{\boldsymbol{k}}}{4\pi} \, T_Q^K(j, \hat{\boldsymbol{k}}) \int_0^\infty d\omega_k \, \mathcal{R}(\Omega_u, \Omega_{u'}; \Omega_l, \Omega_{l'}, \Omega_f; \omega_k, \omega_{k'}) \, S_j(\omega_k, \hat{\boldsymbol{k}}) \ , \qquad (i = 0, 1, 2, 3) \end{aligned}$$

where we adopted the shorthand notation $\Pi_{ab\ldots} \equiv \sqrt{(2a+1)(2b+1)\cdots}$. The various coefficients $C_\mu^{JF}(M)$ represent the projection components of the eigenstates $|\mu M\rangle$ of the magnetic Hamiltonian on the basis of atomic states of the form $|(JI)FM\rangle$. In writing equation (4) we also introduced the redistribution function in the atomic frame of reference,

$$\mathcal{R}(\Omega_u, \Omega_{u'}; \Omega_l, \Omega_{l'}, \Omega_{l''}; \omega_k, \omega_{k'}) \equiv (\epsilon_{uu'} + \mathrm{i}\omega_{uu'}) \left(\Psi_{u'l', l''ul}^{-k, +k'-k} + \bar{\Psi}_{ul, l''u'l'}^{-k, +k'-k} \right) \ . \qquad (5)$$

The transformation of equation (4) to the laboratory frame of reference is formally attained by replacing the redistribution function of equation (5) with the appropriate velocity-dependent function $R(\Omega_u, \Omega_{u'}; \Omega_l, \Omega_{l'}, \Omega_{l''}; \hat{\omega}_k, \hat{\omega}_{k'}; \Theta)$, where $\hat{\omega}_k$ and $\hat{\omega}_{k'}$ are the frequencies of the incoming and outgoing radiation in the laboratory frame, respectively, and Θ is the scattering angle. The task of extending the redistribution function in the laboratory frame to the case of a Λ-type three-term polarized atom has been undertaken in a separate work (R. Casini & R. Manso Sainz 2016; in preparation). In the Appendix, we give the form of such redistribution function in the limit case of *non-coherent lower term*, which applies practically to all the examples presented in Section 3.

It is important to note that the widths of the level u and u' appearing in the redistribution profiles of the form $\Psi^{-k,+k'-k}_{u'l',ful}$ must take into account all possible spontaneous de-excitation processes towards lower terms l, i.e.,

$$\epsilon_u = \frac{1}{2}\sum_l A_{ul} \approx \epsilon_{u'} \ , \tag{6}$$

where, according to our model, the set of lower terms l also includes the final term f.

For some applications, including those presented in the next section, it is necessary to consider atomic models without hyperfine structure, i.e., $I = 0$. In that case, after some straightforward Racah algebra manipulations of equation (4), we find

$$\begin{aligned}
\varepsilon_i^{(2)}(\omega_{k'}, \hat{\boldsymbol{k}}') = {} & \frac{3}{16\pi^3}\mathcal{N}\hbar\,\omega_{k'}^4\,\Pi_{L_u}^2\frac{A_{uf}}{\omega_{uf}^3}\sum_{L_l}\Pi_{L_l}^2 B_{lu} \\
& \times \sum_{J_u J'_u J''_u J'''_u}\ \sum_{J_l J'_l J_f J'_f} \Pi_{J_u J'_u J''_u J'''_u}\,\Pi_{J_l J'_l J_f J'_f}
\begin{Bmatrix} J_u & J_l & 1 \\ L_l & L_u & S \end{Bmatrix}
\begin{Bmatrix} J'_u & J'_l & 1 \\ L_l & L_u & S \end{Bmatrix}
\begin{Bmatrix} J''_u & J_f & 1 \\ L_f & L_u & S \end{Bmatrix}
\begin{Bmatrix} J'''_u & J'_f & 1 \\ L_f & L_u & S \end{Bmatrix} \\
& \times \sum_{\mu_u M_u}\ \sum_{\mu'_u M'_u}\ \sum_{\mu_f M_f} C^{J_u}_{\mu_u}(M_u)\, C^{J''_u}_{\mu_u}(M_u)\, C^{J'_u}_{\mu'_u}(M'_u)\, C^{J'''_u}_{\mu'_u}(M'_u)\, C^{J_f}_{\mu_f}(M_f)\, C^{J'_f}_{\mu_f}(M_f) \\
& \times (\epsilon_{uu'} + \mathrm{i}\omega_{uu'})^{-1} \sum_{\bar{J}_l \bar{J}'_l}\ \sum_{\mu_l M_l}\ \sum_{\mu'_l M'_l} C^{J_l}_{\mu_l}(M_l)\, C^{\bar{J}_l}_{\mu_l}(M_l)\, C^{J'_l}_{\mu'_l}(M'_l)\, C^{\bar{J}'_l}_{\mu'_l}(M'_l) \\
& \times \sum_{KQ}\sum_{K'Q'}\sum_{K_l Q_l}\sum_{qq'}\sum_{pp'} (-1)^{\bar{J}_l - M_l + q' + p'}
\begin{pmatrix} 1 & 1 & K \\ -q & q' & -Q \end{pmatrix}
\begin{pmatrix} 1 & 1 & K' \\ -p & p' & -Q' \end{pmatrix}
\begin{pmatrix} \bar{J}_l & \bar{J}'_l & K_l \\ M_l & -M'_l & -Q_l \end{pmatrix} \\
& \qquad \times \begin{pmatrix} J_u & J_l & 1 \\ -M_u & M_l & q \end{pmatrix}
\begin{pmatrix} J'_u & J'_l & 1 \\ -M'_u & M'_l & q' \end{pmatrix}
\begin{pmatrix} J'''_u & J'_f & 1 \\ -M'_u & M_f & p \end{pmatrix}
\begin{pmatrix} J''_u & J_f & 1 \\ -M_u & M_f & p' \end{pmatrix} \\
& \qquad \times \Pi_{KK'K_l}\, T^{K'}_{Q'}(i, \hat{\boldsymbol{k}}')\, \rho^{K_l}_{Q_l}(\bar{J}_l, \bar{J}'_l) \\
& \times \sum_{j=0}^{3} \oint \frac{d\hat{\boldsymbol{k}}}{4\pi}\, T^K_Q(j, \hat{\boldsymbol{k}}) \int_0^\infty d\omega_k\, \mathcal{R}(\Omega_u, \Omega_{u'}; \Omega_l, \Omega_{l'}, \Omega_f; \omega_k, \omega_{k'})\, S_j(\omega_k, \hat{\boldsymbol{k}}) \ , \qquad (i = 0, 1, 2, 3)
\end{aligned} \tag{7}$$

Finally, in the case of the multi-level atom, there is no dependence of the line profiles on the μ-indices, and so we can use the orthogonality properties of the Hamiltonian eigenvectors (see equations (I.23)) in order to perform the trivial summations over those indices. The expression of the second-order emissivity for this model atom can be derived directly from equation (7) by

imposing the additional conditions $S = 0$ and $L = J$:

$$\varepsilon_i^{(2)}(\omega_{k'}, \hat{\boldsymbol{k}}') = \frac{3}{16\pi^3}\mathcal{N}\hbar\omega_{k'}^4\,\Pi_{J_u}^2\frac{A_{uf}}{\omega_{uf}^3}\sum_{J_l}\Pi_{J_l}^2 B_{lu} \tag{8}$$

$$\times \sum_{M_u M_u'}\sum_{M_l M_l'}\sum_{M_f}\sum_{KQ}\sum_{K'Q'}\sum_{K_l Q_l}\sum_{qq'}\sum_{pp'}(-1)^{J_l - M_l + q' + p'}\begin{pmatrix}1 & 1 & K\\ -q & q' & -Q\end{pmatrix}\begin{pmatrix}1 & 1 & K'\\ -p & p' & -Q'\end{pmatrix}$$

$$\times\begin{pmatrix}J_u & J_l & 1\\ -M_u & M_l & q\end{pmatrix}\begin{pmatrix}J_u & J_l & 1\\ -M_u' & M_l' & q'\end{pmatrix}\begin{pmatrix}J_u & J_f & 1\\ -M_u' & M_f & p\end{pmatrix}\begin{pmatrix}J_u & J_f & 1\\ -M_u & M_f & p'\end{pmatrix}\begin{pmatrix}J_l & J_l & K_l\\ M_l & -M_l' & -Q_l\end{pmatrix}$$

$$\times(\epsilon_{uu'} + \mathrm{i}\omega_{uu'})^{-1}\,\Pi_{KK'K_l}\,T_{Q'}^{K'}(i, \hat{\boldsymbol{k}}')\,\rho_{Q_l}^{K_l}(J_l)$$

$$\times\sum_{j=0}^{3}\oint\frac{d\hat{\boldsymbol{k}}}{4\pi}\,T_Q^K(j, \hat{\boldsymbol{k}})\int_0^\infty d\omega_k\,\mathcal{R}(\Omega_u, \Omega_{u'}; \Omega_l, \Omega_{l'}, \Omega_f; \omega_k, \omega_{k'})\,S_j(\omega_k, \hat{\boldsymbol{k}})\,. \qquad (i = 0, 1, 2, 3)$$

In the next section, we provide examples of the application of this formalism (specifically, of equation (7)) to a few notable Λ-type three-term atoms, namely the Lyβ-Hα system of hydrogen, and the Ca II H-K doublet with the IR triplet (see Table 1).

3. Examples of partial redistribution in Λ-type three-term polarized atoms

As an application of equation (7), we first consider the simplest case of the Λ-type system $1s$-$3p$-$2s$ of H I, which pertains to the formation of the Lyβ and Hα lines, respectively at 102.5 nm and 656.3 nm. Since both lines formed in this restricted Λ-type system have sharp lower levels, the corresponding three-term model atom can indeed be described through the formalism presented above. More specifically, we model the effect of detuning of the UV radiation around the wavelength of the Lyβ line on the intensity and polarization of the Hα line. For this purpose, we assume an ensemble of H I atoms with a pre-assigned distribution of population and atomic polarization in the ground and metastable states. This distribution is derived by solving the statistical equilibrium for the atomic system under prescribed illumination conditions, corresponding to a collimated beam of highly diluted radiation with a Planckian spectrum at $T_{\rm rad} = 20\,000$ K. Under such conditions, the population of the excited $3p\,^2P^\circ$ term is negligible with respect to the populations of the ground and metastable states (by about 9 and 8 orders of magnitude, respectively), and the PRD formalism presented in this work, where the incoherent emission of photons from spontaneous de-excitation of the upper term can be neglected, thus becomes applicable. We also remark that the atomic system so prepared will in general harbor atomic polarization, because of the condition of anisotropic illumination associated with the collimated beam of incident radiation.

Figure 2 shows the scattered radiation produced in this system. The wavelength of the UV incident radiation, which again is monochromatic and unpolarized, is marked by the vertical dashed lines in the Stokes I and Q plots of the Lyβ line. In order to clearly identify the various contributions to the scattered radiation in the system, we assume no incident radiation at the Hα wavelength. Hence, the radiation scattered in the spectral range of Hα is completely due to Raman scattering through virtual excitation of the $3p\,^2P^\circ$ term by the UV radiation.

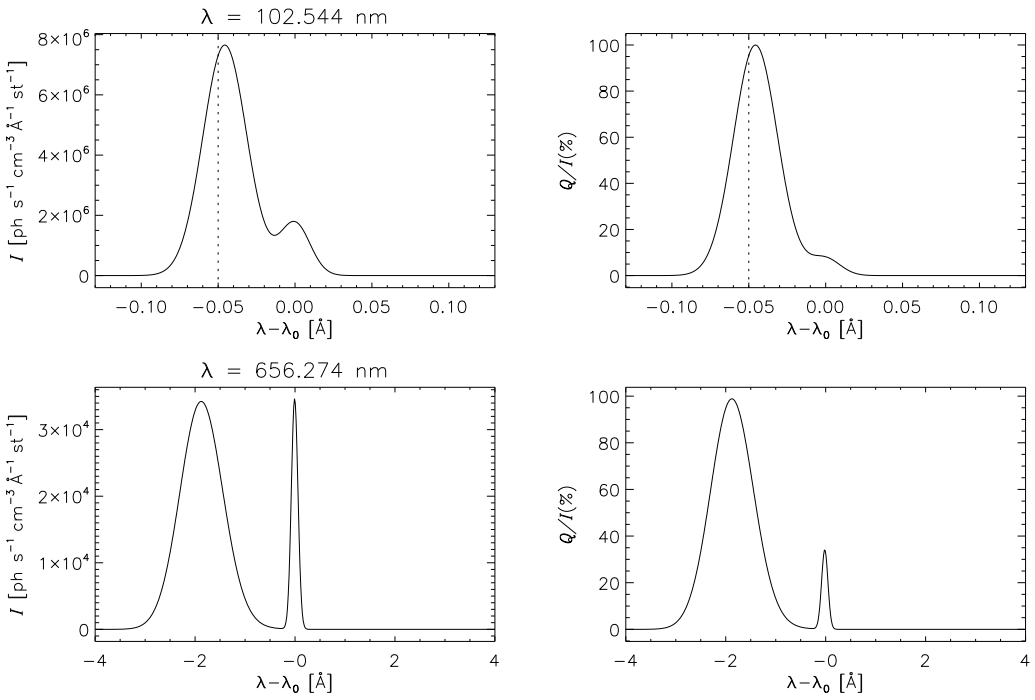

Fig. 2.— Stokes I and Q emission profiles of the H I Lyβ (top panels) and Hα (bottom panels) lines, respectively at 102.5 nm and 656.3 nm. The model is for the 90-degree scattering of a collimated beam of radiation by a plasma with temperature $T = 1000\,\mathrm{K}$, and no magnetic field. The intensity of the incident radiation field corresponds to a Planckian spectrum at $T_{\mathrm{rad}} = 20\,000\,\mathrm{K}$. The incident UV radiation (monochromatic and unpolarized) is nearly resonant with the Lyβ transition, with a detuning of $-0.05\,\mathrm{\AA}$ (vertical dashed lines in the top panels). We note the presence of a secondary contribution in the scattered radiation, which is perfectly resonant with the natural wavelength of the line. The intensity profile amplitude is expressed as number of scattered photons per unit intervals of time, emitting volume, wavelength, and solid angle, assuming a reference gas density $\mathcal{N} = 10^{12}\,\mathrm{cm}^{-3}$ for the emitting volume.

We note that the scattered radiation in the Lyβ line is dominated by the coherent component centered around the wavelength of the monochromatic UV incident radiation. However, because of the relatively large Doppler width compared to the size of the detuning, a small contribution, resonant with the natural transition of the line and blended with the coherent component, is also present in this case. In contrast, the emission in Hα shows these same two contributions well separated. In fact, if we indicate with $\delta\lambda_{ul}$ the detuning of the incident radiation in the Λ-type system, for the final branch of the scattering process

$$\delta\lambda_{uf} = \left(\frac{\lambda_{uf}}{\lambda_{ul}}\right)^2 \delta\lambda_{ul}\ . \tag{9}$$

Because in Figure 2 the detuning from the Lyβ resonance is $\delta\lambda_{ul} = -0.05\,\mathrm{\AA}$, the coherent component

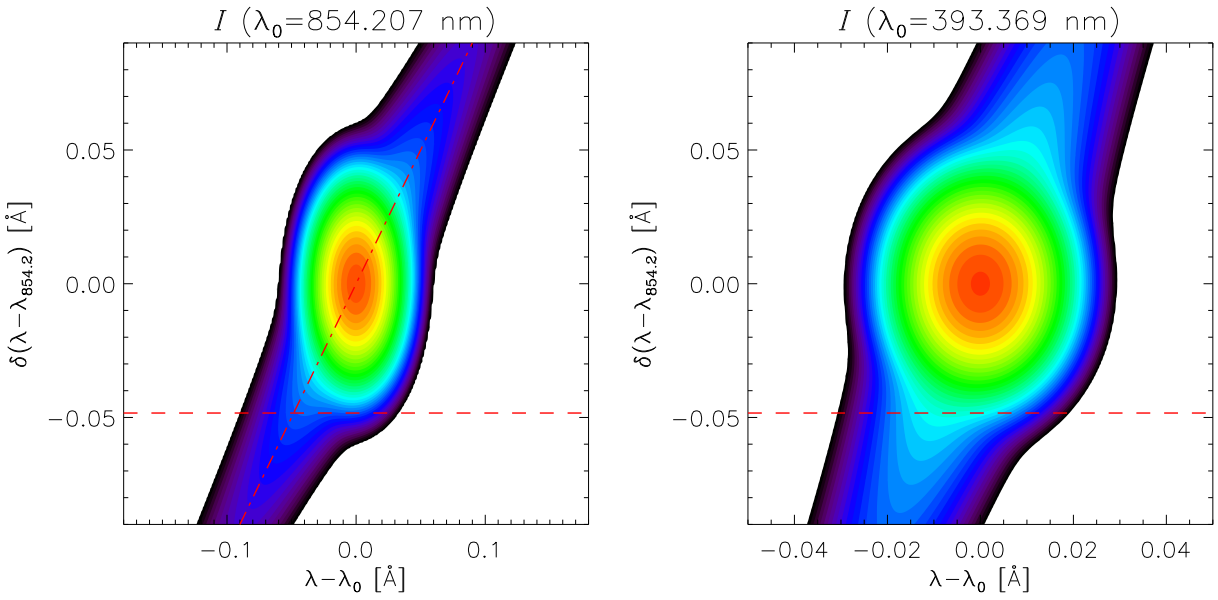

Fig. 3.— Contour plots of the scattered intensity of the IR line at 854.2 nm (left) and the K line at 393.4 nm (right) of Ca II, as a function of wavelength across the line spectral ranges (x axes), and of the detuning of the incident monochromatic IR radiation around the 854.2 nm resonance wavelength (y axis). The scattering configuration is the same as for Figure 2, but for an incident radiation with a Planckian spectrum at $T_{\rm rad} = 5000\,{\rm K}$. The diagonal dash-dotted line in the left panel tracks the location of the monochromatic illumination with respect to the intensity profile of the scattered 854.2 nm line, for the various values of detuning. The horizontal dashed lines locate the value of the detuning of the monochromatic IR incident radiation adopted for the calculation of the emission profiles shown in Figure 4.

in Hα occurs with a wavelength shift from resonance given by $\delta\lambda_{uf} \approx -2.05\,$Å. As this is larger than the Doppler width corresponding to the assumed plasma temperature (which instead scales linearly with the wavelength of the transition), the coherent and resonant contributions in the Hα line appear completely separated. We also note that the line profiles of both transitions are 100% linearly polarized at the frequency of coherent re-emission, as it is to be expected in the wings of S-P transitions. Finally, we point out that the wavelength integrated intensity profiles of Figure 2, which give the total numbers of photons emitted in the Lyβ and Hα lines, are in exactly the same ratio as the Einstein A-coefficients of the two transitions, which is also to be expected.

Next, we consider the more complex atomic system of Ca II, leading to the formation of the H and K lines around 395 nm and the IR triplet around 858 nm. We model the effect of detuning in the two cases where the monochromatic incident radiation is located in the proximity of either one or the other of the two transitions. We consider the same scattering configuration as in the previous example, with the exception of the temperature of the incident radiation, for which we assume instead a Planckian spectrum at $T_{\rm rad} = 5000\,{\rm K}$.

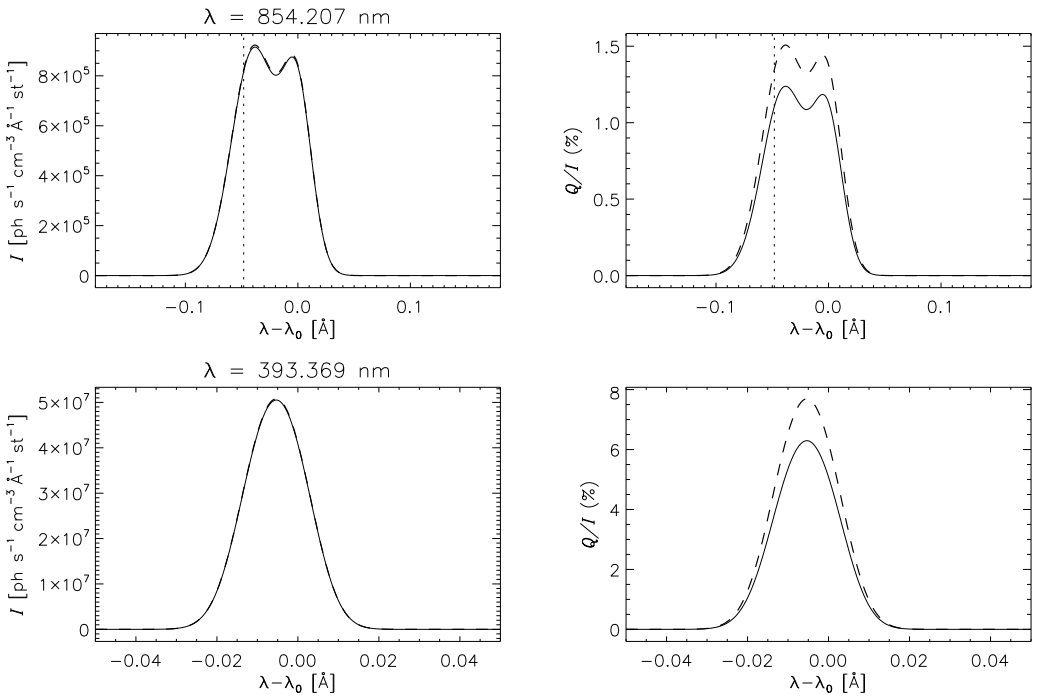

Fig. 4.— Stokes I and Q emission profiles of the IR 854.2 nm line (top panels) and the K line at 393.4 nm (bottom panels) of Ca II, for the same scattering model adopted for Figure 3. These profiles correspond to the detuning of the incident radiation from the 854.2 nm wavelength resonance identified by the horizontal dashed lines in the contour plots of Figure 3. Hence, the Stokes I profiles represent the horizontal cut of those contour plots for the corresponding value of the detuning of the incident IR radiation. The profiles shown with dashed curves correspond to the case when the atomic polarization of the metastable state of the Ca II system is neglected.

Figure 3 shows contour plots of the scattered Stokes I emission profiles (wavelength along the x axis) of the IR line at 854.2 nm (left) and the K line at 393.4 nm (right) of Ca II, as a function of the frequency of a monochromatic illumination (wavelength along the y axis) varying within a spectral range of 0.18 Å around the 854.2 nm resonance wavelength. Each horizontal slice of those plots thus corresponds to the scattered line intensity profile for the corresponding value of the detuning from the 854.2 nm resonance. Again, we assume no direct illumination of the Ca II K line for this modeling, and so the emitted radiation in that line is purely produced by Raman scattering induced via virtual excitation of the upper state of the K line by the IR illumination. In particular, this allows us to represent the scattered radiation in both lines via the contour plots of Figure 3, as a function of only one detuning parameter. The observed spectral spread of the re-emitted radiation along the x axis is produced by Doppler redistribution, corresponding to the plasma temperature of 1000 K. Also for this model we assumed a zero magnetic field. In such case, the wavelength dependence of the Stokes Q polarization qualitatively resembles closely that of the

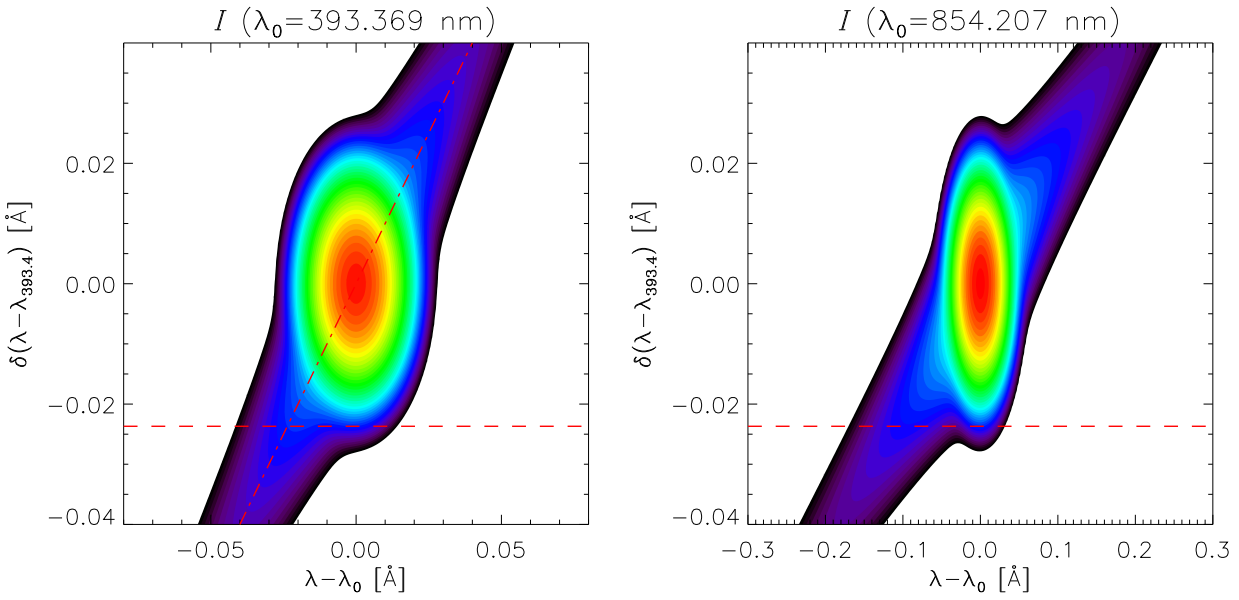

Fig. 5.— Same as Figure 3, but for an inverted role of the two transitions, where the monochromatic incident radiation this time is tuned across the spectral range of the K line centered at 393.4 nm, with no radiation directly exciting the IR line at 854.2 nm. The horizontal dashed lines locate the value of the detuning of the monochromatic UV incident radiation adopted for the calculation of the emission profiles shown in Figure 6.

intensity profiles (see also Figure 4, and therefore we omitted showing contour plots also of Stokes Q.

The dash-dotted diagonal line in the left plot tracks the wavelength of the monochromatic IR incident radiation as it scans across the spectral interval around the 854.2 nm resonance wavelength. As the detuning from the 854.2 nm transition (which is read on the y axis) decreases in absolute value, the signal of the scattered radiation remains initially fully coherent with the frequency of the incident radiation, while at the same time it increases in strength. In fact, for values of the detuning larger than ~ 0.06 Å in absolute value, the virtual energy levels of the upper term attained during the scattering process lie outside the energy band corresponding to the thermal line width of the upper term. Then there is no energy overlap leading to quantum interference between these levels and the atomic Hamiltonian eigen-levels of the upper term, and the scattering is purely coherent in both the Ca II K and 854.2 nm lines. This process corresponds to Rayleigh scattering of the monochromatic incident radiation, and the frequency spread observed in the scattered radiation is dominated by the Doppler redistribution corresponding to the plasma temperature.

However, at about 0.06 Å from resonance, the signal of the non-coherent contribution at the resonance wavelength of the 854.2 nm line begins to appear, becoming the dominant term of the scattered radiation in an interval of about ± 0.045 Å around the resonance. The radiation emitted in the K line, which is produced by Raman scattering towards the Ca II ground state, is also

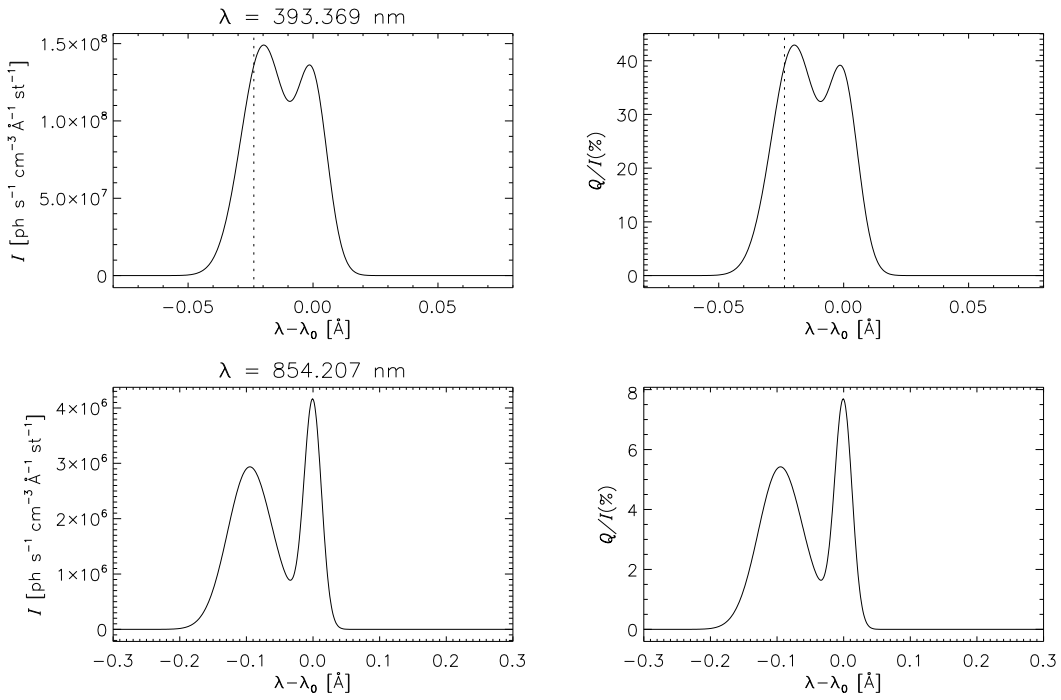

Fig. 6.— Stokes I and Q emission profiles of the K line at 393.4 nm (top panels) and the IR 854.2 nm line (bottom panels) of Ca II, for the same scattering model adopted for Figure 3, but in the case where the monochromatic incident radiation is tuned around the K line resonance wavelength. We note how in this case the profiles of both lines can become visibly double-peaked, as a consequence of equation (9). These profiles correspond to the cut of the contour plots of Figure 5 for the value of the detuning of the monochromatic UV incident radiation identified by the horizontal dashed lines.

dominated by the resonant contribution at 393.4 nm approximately within the same interval of detuning of the IR illumination, although the profiles of this line never become double-peaked. This can be understood if we recall equation (9), and it is clearly illustrated by Figure 4, which shows the Stokes I and Q emission profiles (solid curves) for a detuning of ~ 0.05 Å from the 854.2 nm resonance wavelength (horizontal slice of the contour plots of Figure 3 identified by the dashed lines). Overplotted on these profiles, with the dashed curves, we show the same case where the contribution of the atomic polarization in the metastable state of Ca II is neglected. As we see from comparing the two sets of profiles, the linear polarization of the scattered radiation in both Ca II K and 854.2 nm lines is larger in that case.

Figures 5 and 6 are analogous to Figures 3 and 4, for the case where the monochromatic incident radiation is tuned across the resonance wavelength of the K line at 393.4 nm instead, with no radiation directly exciting the IR transition at 854.2 nm. As evidenced by Figure 6, in this case the profiles of both lines can become double-peaked (for values of the detuning from resonance larger than ~ 0.02 Å in absolute value), in virtue of the separation between the coherent and resonant

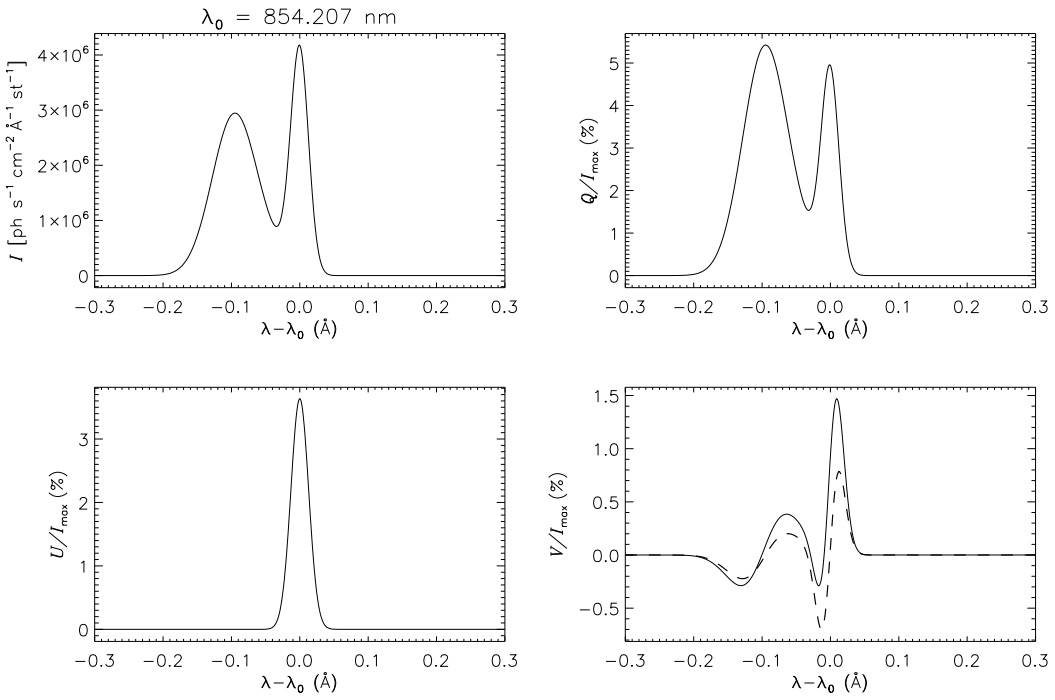

Fig. 7.— Stokes emission profiles of the Ca II K line, with the same detuning of the UV radiation around the K line resonance as for Figure 6, but in the case where a magnetic field with $B = 5\,\mathrm{G}$ directed towards the observer is also present. We note the manifestation of the Hanle effect polarization in both Stokes Q and U, in the resonant core of the line. The dashed curve in the panel for Stokes V represents the weak-field approximation to the circular polarization signal, computed through the first derivative of Stokes I, assuming the LS-coupling value for the effective Landé factor of the line, $g_{\mathrm{eff}} \approx 1.1$.

contributions satisfying equation (9).

When a magnetic field is present, the profiles evidently become more complicated, although some general conclusions can be drawn from the example presented in Figure 7. This shows the full Stokes profiles of the Ca II IR line at 854.2 nm under the same illumination conditions of Figure 6, but with the addition of a magnetic field of 5 G directed towards the observer (i.e., normal to the direction of the incident radiation). Because the magnetic field strength is comparable to the Hanle critical field for the upper level $^2P_{3/2}$ of the Ca II 854.2 nm and K lines ($B_{\mathrm{Hanle}} \approx \epsilon_u/(0.8794 \times 10^7\, g_u) \approx 6.7\,\mathrm{G}$, where $g_u \approx 1.333$ is the Landé factor of the $^2P_{3/2}$ level, and ϵ_u is calculated via equation (6)), one expects that the Stokes profiles will show evidence of Hanle-effect depolarization. Indeed, comparing the bottom panels of Figure 6 with the top panels of Figure 7, we see that the intensity profile is practically unaffected by the presence of a weak magnetic field, whereas the resonant component of Stokes Q shows a depolarization with respect to the zero-field case, and accordingly a signal in Stokes U appears. It is important to observe that the Stokes U

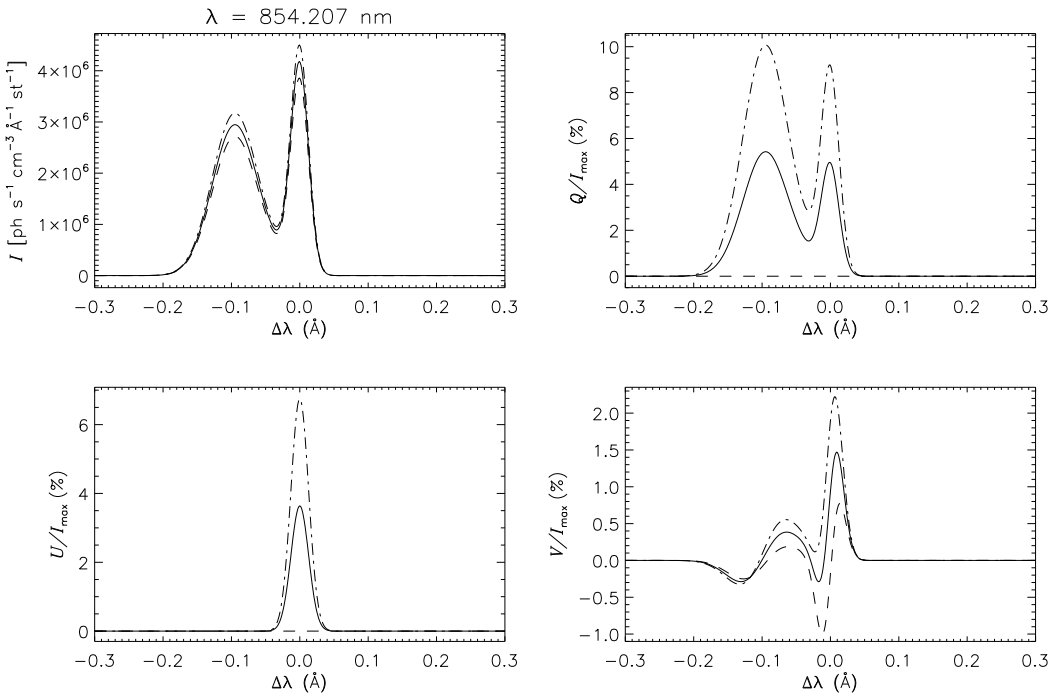

Fig. 8.— Stokes profiles of the Ca II line at 854.2 nm, for the same scattering configuration and magnetic model of Figure 7, and different conditions of polarization of the monochromatic UV incident radiation in the proximity of the Ca II K line: unpolarized (solid curves; identical to the case of Figure 7); fully linearly polarized along the LOS (dashed curves); fully linearly polarized perpendicularly to the LOS (dash-dotted curves).

signal manifests itself strictly in the resonant core of the line, which is also where the depolarization of Stokes Q occurs. This is to be expected, since the Hanle effect is a manifestation of the relaxation of atomic coherence as the energy degeneracy of the atomic Hamiltonian eigen-levels is lifted by the applied magnetic field.

We also note that the shape of Stokes V is not quite reproduced by the weak-field approximation of the circular polarization signal (dashed curve in the bottom-right panel of Figure 7), despite the very small strength of the applied field, and the fact that all polarization effects due to level interference induced by the magnetic field, such as Stokes-V asymmetries associated with atomic orientation, are completely negligible in this case, because of the relatively large fine structure separation between the $J = 1/2, 3/2$ levels of the upper term. Therefore, the net circular polarization observed in Figure 7 is a manifestation of the effects of partial redistribution on the circular polarization of the scattered light.

All previous examples were calculated assuming an unpolarized beam of incident radiation. Figure 8 shows instead the Stokes profiles of the Ca II 854.2 nm line for the same scattering configuration and magnetic model as in the example of Figure 7, but under different conditions of

polarization of the incident UV radiation. More precisely, the atomic system is still prepared assuming the same flat and unpolarized radiation field as in all previous examples, and only the incident beam of radiation used in equation (7) is now assumed to be linearly polarized. The solid curves represent the case of unpolarized incident radiation as a reference, which are identical to those shown in Figure 7. The other curves represent instead the cases of fully linearly polarized radiation with $Q/I = +1$ (polarization along the LOS; dashed curves) and $Q/I = -1$ (polarization perpendicular to the LOS; dash-dotted curves). When the incident beam of radiation is linearly polarized along the LOS, the linear polarization of the scattered radiation is practically completely suppressed (in fact, by approximately six orders of magnitude compared to the unpolarized case), as it can be expected also on the basis of simple classical arguments (Mitchell & Zemansky 1934).

As a concluding remark, we want to point out that, while the atomic polarization produced by the anisotropy of the incident radiation is fully accounted for in the modeling examples presented in this work, all those examples are realized under physical conditions where the atomic coherence in the lower terms is practically negligible. This is either because the magnetic field is absent (Figures 2 to 6), or because the magnetic strength is above the critical value for the Hanle effect of the lower term (Figures 7 and 8), yet small enough not to induce any J-J' level interference via the Paschen-Back effect. The realization of this range of physical conditions allows us to adopt a reduced form of the redistribution function for the polarized atom introduced in Casini et al. (2014), which corresponds to a direct generalization to the three-term atom of the $R_{\rm II}$ function adopted elsewhere in the PRD literature (e.g., Belluzzi & Trujillo Bueno 2014).

We thank Tanausú del Pino Alemán (Instituto de Astrofísica de Canarias; IAC) for helpful discussions during the initial testing of the code with which the results of this paper were produced. We also thank Rebecca Centeno Elliot (HAO) and Javier Trujillo Bueno (IAC) for reading the manuscript and for providing helpful comments and suggestions. RMS acknowledges partial support by the Spanish Ministry of Economy and Competitiveness (project AYA2010-18029), and the support of the HAO Visitor Program, which made this work possible.

We dedicate this work to the memory of David G. Hummer (1934-2015), who greatly contributed to the field of frequency redistribution. David, who for many years of his active career was a vital collaborator of HAO and NCAR, as witnessed by his many works published together with HAO scientists, passed away on December 17, while this paper was receiving the final strokes.

A. Redistribution function of the Λ-type three-term atom in the laboratory frame

In the case of infinitely sharp lower levels (s.l.l.), and assuming that the initial term of the Λ-type transition is *non-coherent* (i.e., $\rho_{ll'} = \delta_{ll'}\rho_{ll}$), the redistribution function for the Λ-type three-term polarized atom, expressed in the laboratory reference frame, is given by

$$R(\Omega_u,\Omega_{u'};\Omega_l,\Omega_f;\hat{\omega}_k,\hat{\omega}_{k'};\Theta)_{\rm s.l.l.} = \frac{2\pi}{\Delta^2\, S\xi_l\xi_f}\exp\left[-\frac{(\hat{\omega}_k-\hat{\omega}_{k'}+\omega_{lf})^2}{\Delta^2}\right] \times\left[W\left(\frac{\kappa^+ v_{ul}+\kappa^- w_{uf}}{S\xi_l\xi_f},\frac{a_u}{S\xi_l\xi_f}\right)+\overline{W}\left(\frac{\kappa^+ v_{u'l}+\kappa^- w_{u'f}}{S\xi_l\xi_f},\frac{a_{u'}}{S\xi_l\xi_f}\right)\right], \tag{A1}$$

where

$$W(v,a) = \frac{1}{\pi}\int_{-\infty}^{+\infty} dp\ \frac{\mathrm{e}^{-p^2}}{a+\mathrm{i}(p-v)} = H(v,a) + \mathrm{i}\,L(v,a)\ , \tag{A2}$$

with $H(v,a)$ and $L(v,a)$ being respectively the Voigt and Faraday-Voigt functions. The full derivation of the above result is contained in an upcoming paper (R. Casini & R. Manso Sainz 2016; in preparation).

For each scattering event, Θ is the angle between the propagation directions of the incoming and outgoing photons. We introduced accordingly the associated quantities

$$C = \cos\Theta\ , \qquad S = \sin\Theta\ . \tag{A3}$$

Next we defined

$$\Delta = (\Delta_{ul}^2 + \Delta_{uf}^2 - 2C\Delta_{ul}\Delta_{uf})^{1/2}\ , \tag{A4}$$

$$\xi_l = \Delta_{ul}/\Delta\ , \qquad \xi_f = \Delta_{uf}/\Delta\ , \tag{A5}$$

where Δ_{mn} is the Doppler width of the transition between the atomic states m and n, with Bohr frequency ω_{mn}. We introduced the normalized frequency variables

$$v_{mn} = (\hat{\omega}_k - \omega_{mn})/\Delta\ , \qquad w_{mn} = (\hat{\omega}_{k'} - \omega_{mn})/\Delta\ , \tag{A6}$$

where the incoming and outgoing radiation frequencies, $\hat{\omega}_k$ and $\hat{\omega}_{k'}$, are expressed in the laboratory frame of reference. We also introduced normalized damping parameters associated with the inverse lifetimes of the transition levels, using the same "reduced" Doppler width of equation (A4),

$$a_m = \epsilon_m/\Delta\ . \tag{A7}$$

Finally, we introduced the transitions' "weights"

$$\kappa^{\pm} = \tfrac{1}{2}\left[1 \pm (\xi_f^2 - \xi_l^2)\right]\ . \tag{A8}$$

REFERENCES

Belluzzi, L., & Trujillo Bueno, J. 2011, ApJ, 743, 3

Belluzzi, L., & Trujillo Bueno, J. 2013, A&A, 564, 16

Bommier, V. 1997, A&A, 328, 726

Casini, R., & Manso Sainz, R. 2005, ApJ, 624, 1025

Casini, R., Landi Degl'Innocenti, M., Manso Sainz, R., Landi Degl'Innocenti, E., & Landolfi, M.. 2014, ApJ, 791, 94

Gandorfer, A. 2000, The Second Solar Spectrum: A high spectral resolution polarimetric survey of scattering polarization at the solar limb in graphical representation. Volume I: 4625Å to 6995Å (Zurich: vdf Hochschulverlag)

Gandorfer, A. 2002, The Second Solar Spectrum: A high spectral resolution polarimetric survey of scattering polarization at the solar limb in graphical representation. Volume II: 3910Å to 4630Å (Zurich: vdf Hochschulverlag)

Gandorfer, A. 2005, The Second Solar Spectrum: A high spectral resolution polarimetric survey of scattering polarization at the solar limb in graphical representation. Volume III: 3160Å to 3915Å (Zurich: vdf Hochschulverlag)

Landi Degl'Innocenti, E. 1984, Sol. Phys., 91, 1

Landi Degl'Innocenti, E. 1998, Nature, 392, 256

Landi Degl'Innocenti, E., & Landolfi, M. 2004, Polarization in Spectral Lines (Dordrecht: Springer)

Manso Sainz, R., & Trujillo Bueno, J. 2001, in Advanced Solar Polarimetry, Theory, Observation, and Instrumentation,20th NSO/Sacramento Peak Summer Workshop, ASP Conference Proceedings, 236, ed. M. Sigwarth (San Francisco: ASP), 213

Manso Sainz, R., & Trujillo Bueno, J. 2003, Phys. Rev. Lett., 91, 111102

Mitchell, A. C. G., & Zemansky, M. W. 1934, Resonance Radiation and Excited Atoms (Cambridge: Cambridge)

Sampoorna, M., Nagendra, K. N., & Stenflo, J. O. 2013, ApJ, 770, 92

Smitha, H. N., Nagendra, K. N., Stenflo, J. O., Bianda, M., Sampoorna, M., Ramelli, R., & Anusha, L. S. 2013, A&A, 541, 24

Stenflo, J. O. 1980, A&A, 84, 68

Stenflo, J. O. 1997, A&A, 324, 344

Stenflo, J. O., & Keller, C. U. 1996, Nature, 382, 588

Stenflo, J. O., & Keller, C. U. 1997, A&A, 321, 927

Stenflo, J. O., Baur, T. G., & Elmore, D. F. 1980, A&A, 84, 60

Stenflo, J. O., Twerenbold, D., Harvey, J. W. 1983a, A&AS, 52, 161

Stenflo, J. O., Twerenbold, D., Harvey, J. W., Brault, J. W. 1983b, A&AS, 54, 505

Stenflo, J. O., Keller, C. U., & Gandorfer, A. 2000, A&A, 355, 789

Trujillo Bueno, J., & Landi Degl'Innocenti, E. 1997, ApJ, 482, L183

Trujillo Bueno, J., Landi Degl'Innocenti, E., Collados, M., Merenda, L., & Manso Sainz, R. 2002, Nature, 415, 403

Wiehr, E. 1975, A&A, 38, 303

This preprint was prepared with the AAS LaTeX macros v5.2.